Electronic Supplementary Material for

Design Framework for Mechanically Tunable Soft Biomaterial Composite Enhanced by Modified Horseshoe Lattice Structures

Dong Wang [a,b*], Yi Xiong [b], Biao Zhang [b,c], Yuan-Fang Zhang [b], David Rosen [b, d], Qi Ge [b, e*]

[a] Robotics Institute, School of Mechanical Engineering, Shanghai Jiao Tong University, Shanghai 200240, China.

[b] Digital Manufacturing and Design Centre, Singapore University of Technology and Design, Singapore 487372, Singapore

[c] Xi'an Institute of Flexible Electronics and Xi'an Key Laboratory of Biomedical Materials & Engineering, Northwestern Polytechnical University (NPU), Xi'an710072, Shaanxi, China

[d] The George W. Woodruff School of Mechanical Engineering, Georgia Institute of Technology, 813 Ferst Drive, NW, Atlanta, GA 30332-0405, United States

[e] Department of Mechanical and Energy Engineering, Southern University of Science and Technology, Shenzhen 518055, China

[*]To whom correspondence may be addressed. Email: wang_dong@sjtu.edu.cn (D. W.); geq@sustech.edu.cn (Q. G.).

Keywords:

reinforced hydrogel, highly stretchable, negative Poisson effect, 3D printing, periodical lattice structure

I: Theoretical derivation of single horseshoe structure under axial force, shear force and moment

The axial force N, the shear force Q and the bending moment M at any cross section, and they can be calculated by following equations:

$$N = EA\varepsilon,\ M = EI(1+\varepsilon)\frac{\mathrm{d}\varphi}{\mathrm{d}s} = EI\frac{\mathrm{d}\varphi}{\mathrm{d}S}, \tag{1}$$

with Young's modulus E, the cross-section area A ($A = w\cdot d$) of the modified horseshoe microstructure, and the second area moment I ($I = w^3 d/12$). d represents the thickness of the structure in Z direction. The axial force N, the shear force Q and the bending moment M satisfy the following equilibrium equations:

$$\frac{\mathrm{d}N}{\mathrm{d}s} + \frac{Q}{r} = 0,\ -\frac{N}{r} + \frac{\mathrm{d}Q}{\mathrm{d}s} = 0,\ \frac{\mathrm{d}M}{\mathrm{d}s} = Q. \tag{2}$$

Based on the loading condition shown in Fig. 3(c), the axial and shear forces can be calculated as:

$$N = F_x\cos\theta + F_y\sin\theta,\ Q = F_x\sin\theta - F_y\cos\theta. \tag{3}$$

Substituting Eqs. (2) and (3) into Eqs. (1), ε and $\mathrm{d}^2\varphi/\mathrm{d}S^2$ can be rewritten as:

$$\varepsilon = (F_x\cos\theta + F_y\sin\theta)/EA \text{ and } \frac{\mathrm{d}^2\varphi}{\mathrm{d}S^2} = \frac{\left(EA+F_x\cos\theta+F_y\sin\theta\right)\cdot\left(F_x\sin\theta-F_y\cos\theta\right)}{EI\cdot EA}. \tag{4}$$

In the undeformed arc, $\mathrm{d}S = R\mathrm{d}\alpha$ and $\mathrm{d}^2\varphi/\mathrm{d}S^2 = \frac{1}{R^2}\cdot\mathrm{d}^2\varphi/\mathrm{d}\alpha^2$. Therefore, we have

$$\frac{\mathrm{d}^2\theta}{\mathrm{d}\alpha^2} = \frac{R^2\cdot\left(EA+F_x\cos\theta+F_y\sin\theta\right)\cdot\left(F_x\sin\theta-F_y\cos\theta\right)}{EI\cdot EA}. \tag{5}$$

By using the relation $\mathrm{d}\left[(\frac{\mathrm{d}\theta}{\mathrm{d}\alpha})^2\right]\Big/\mathrm{d}\theta = 2\frac{\mathrm{d}^2\theta}{\mathrm{d}\alpha^2}$, Eq. (5) can be rearanged as:

$$\mathrm{d}\left[\left(\frac{\mathrm{d}\theta}{\mathrm{d}\alpha}\right)^2\right] = 2\cdot\frac{R^2\cdot\left(EA+F_x\cos\theta+F_y\sin\theta\right)\cdot\left(F_x\sin\theta-F_y\cos\theta\right)}{EI\cdot EA}\cdot\mathrm{d}\theta. \tag{6}$$

Conducting integration on both sides, $\left(\mathrm{d}\theta/\mathrm{d}\alpha\right)^2$ can be calculated as:

$$(\frac{\mathrm{d}\theta}{\mathrm{d}\alpha})^2 = -\frac{R^2\cdot\left[\left(F_x^{\,2}-F_y^{\,2}\right)\cos 2\theta + 4EAF_y\sin\theta + 4F_x\cos\theta\left(EA+F_y\sin\theta\right)\right]}{2EA\cdot EI} + C \tag{7}$$

where C is a constant to be determined by boundary conditions.

As shown in Fig. 3(c), the moment at $\theta = \gamma$ can be balanced by the moments generated by F_x and F_y at the left end of the half modified horseshoe microstructure:

$$M\big|_{\theta=\gamma} = F_x(-L\sin\beta + l_y) - F_y(L\cos\beta + l_x), \tag{8}$$

where l_x and l_y are the distance between the two ends of the deformed arc in the x and y directions. Because $\varphi=\theta-\alpha$, $\mathrm{d}S=R\mathrm{d}\alpha$ and $\mathrm{d}s=(1+\varepsilon)\mathrm{d}S$, $\mathrm{d}\varphi/\mathrm{d}s$ can be calculated as:

$$\frac{\mathrm{d}\varphi}{\mathrm{d}s}=\frac{1}{(1+\varepsilon)}\left(\frac{\mathrm{d}\theta}{R\mathrm{d}\alpha}-\frac{1}{R}\right). \tag{9}$$

Therefore, the bending moment M in Eq. (1) can be expressed in terms of $\mathrm{d}\theta/\mathrm{d}\alpha$:

$$M=\frac{EI}{R}\left(\frac{\mathrm{d}\theta}{\mathrm{d}\alpha}-1\right). \tag{10}$$

$\mathrm{d}\theta/\mathrm{d}\alpha$ can then be expressed as:

$$\frac{\mathrm{d}\theta}{\mathrm{d}\alpha}=\frac{M\cdot R}{EI}+1. \tag{11}$$

Based on the boundary condition in Eq. (8), $\mathrm{d}\theta/\mathrm{d}\alpha\big|_{\theta=\gamma}$ can be computed:

$$\mathrm{d}\theta/\mathrm{d}\alpha\big|_{\theta=\gamma}=\frac{\left[F_x(-L\sin\beta+l_y)-F_y(L\cos\beta+l_x)\right]\cdot R}{EI}+1. \tag{12}$$

Substituting Eq. (12) into Eq. (7), the constant C can be calculated as:

$$\begin{aligned}C=&\left[-1+\frac{R\left(F_yl_x-F_xl_y+F_yL\cos\beta+FxL\sin\beta\right)}{EI}\right]^2\\&+R^2\frac{\left(F_x{}^2-F_y{}^2\right)\cos2\gamma+4EAF_y\sin\gamma+4F_x\cos\gamma\left(EA+F_y\sin\gamma\right)}{2EA\cdot EI},\end{aligned} \tag{13}$$

where C is a function of two unknowns, l_x and l_y. Thus, based on Eq. (7), $\mathrm{d}\theta/\mathrm{d}\alpha$ can be computed as:

$$\frac{\mathrm{d}\theta}{\mathrm{d}\alpha}=f\left(\theta,l_x,l_y\right), \text{ with}$$

$$f(\theta,l_x,l_y)=\sqrt{-\frac{R^2\cdot\left[\left(F_x{}^2-F_y{}^2\right)\cos2\theta+4EAF_y\sin\theta+4F_x\cos\theta\left(EA+F_y\sin\theta\right)\right]}{2EA\cdot EI}+C}. \tag{14}$$

After rearranging the first equation in Eq. (14), one can integrate the rearranged equation on both sides:

$$\int_{\theta=\beta}^{\theta=\gamma}\frac{\mathrm{d}\theta}{f(\theta,l_x,l_y)}=\int_{\alpha=-\alpha_0}^{\alpha=\alpha_0}\mathrm{d}\alpha. \tag{15}$$

The horizontal and vertical distances l_x and l_y can be calculated as $l_x=\int\cos\theta\mathrm{d}s$ and $l_y=\int\sin\theta\mathrm{d}s$. Recall that $\mathrm{d}s=(1+\varepsilon)\mathrm{d}S$, $\mathrm{d}S=R\mathrm{d}\alpha$, and $\mathrm{d}\alpha=\mathrm{d}\theta\big/f\left(\theta,l_x,l_y\right)$, therefore l_x and l_y can be computed as

$$l_x = \int_{\beta}^{\gamma} \frac{R(1+\varepsilon)\cos\theta}{f(\theta, l_x, l_y)} \mathrm{d}\theta, \text{ and} \tag{16}$$

$$l_y = \int_{\beta}^{\gamma} \frac{R(1+\varepsilon)\sin\theta}{f(\theta, l_x, l_y)} \mathrm{d}\theta . \tag{17}$$

Here, based on Eq. (4), $\varepsilon = -(F_x \cos\theta + F_y \sin\theta) / EA$. In addition, the geometric compatibility requires:

$$L\sin\beta + L\sin\gamma + l_y = 0 . \tag{18}$$

By using the four equations Eqs. (15)-(18), the four unknown β, γ, l_x, l_y can be solved.

II: Turning of the theoretically predicted stress-strain curve

It should be noted that in Fig 5a, the theoretical curve can only predict the deformation of the rectangular horseshoe lattice as the strain < ~150%, as shown in the following figure. After the stress reaches a critical value σ_c , the theoretical model predicts that the periodical unit will tend to rotate to resist the increasing stress (shown by the inset figures). The strain will decrease instead with increasing stress. However, the experiments were conducted under strain control mode and exceeding rotation of the unit is limited due to the constraints on the transverse direction. Thus large discrepancy exists between experiments and theoretical modeling after $\sigma > \sigma_c$. This behavior has not been found in the theoretical modeling of the triangular lattice structure.

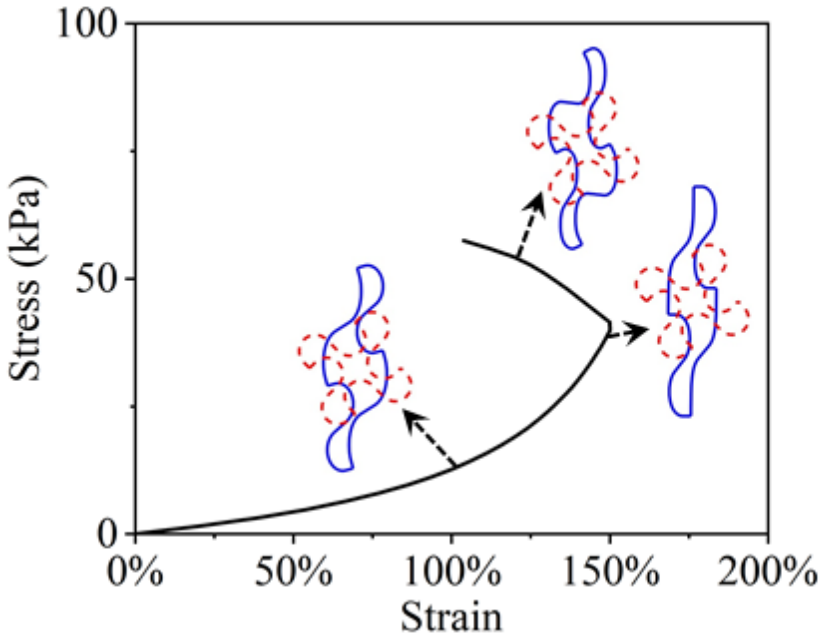

Fig. S1. Theoretical predicted stress-strain curve for the rectangular lattice structure.

III: Bonding between the lattice and hydrogel

From our experimental results, we found that the fabricated hydrogels with 3D printed lattice structures break in the hydrogel region rather than at the interface after being stretched, suggesting that the interface between the hydrogel and the lattice structures is reasonably tough. So we believe that water molecules do not decrease the bonding strength between reinforcement lattice and hydrogel matrix. We attribute the strong interfacial bonding to covalent bonds between the hydrogels and VeroCyan as shown by the following figure. The surfaces of the printed lattice structures still have unreacted acrylate-based monomers, which covalently bond the unreacted double bonds on acrylamide or PEGDA in the hydrogel precursor upon UV irradiation.

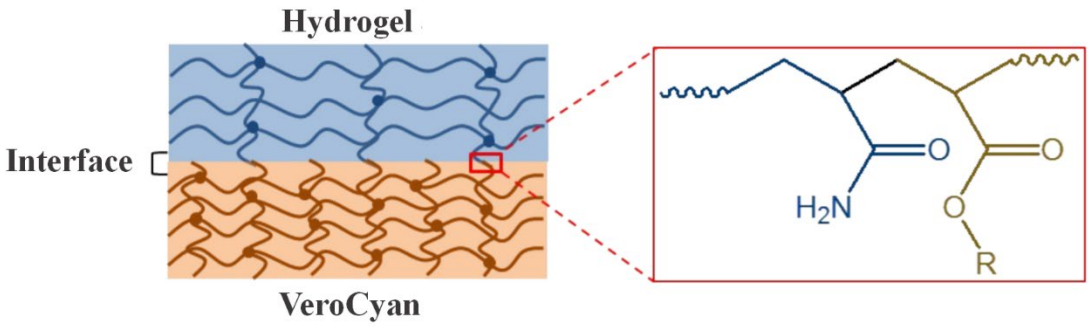

Fig. S2. The proposed bonding mechanism between hydrogel and VeroCyan.